Hot-electron generation in copper and photopumping of cobalt

G. Pretzler, Th. Schlegel, and E. Fill
Max-Planck-Institut für Quantenoptik, D-85748 Garching, Germany

D. Eder
Lawrence Livermore National Laboratory, Livermore, California 94550
(Received 20 March 2000)

Hot electrons generated upon interaction of *p*-polarized 130 fs laser pulses with copper and penetrating into the target material are characterized with respect to their energy distribution and directionality. ''Experimental'' data are obtained by comparing the rear-side x-ray emission from layered targets with Monte Carlo electron-photon transport simulations. Theoretical electron energy distributions are derived by means of a one and a half–dimensional particle-in-cell code. Both sets of data consist of a two-temperature distribution of electrons propagating in a direction almost perpendicular to the target surface. The ''experimental'' data contain a considerably higher population of the lower temperature electrons. The discrepancy is explained by the intensity distribution of the laser spot. The results are used to design an experiment for demonstrating photopumping of cobalt with copper $K\alpha$ radiation. A 10 μm copper foil is backed with 1 mm of polyethylene (PE) followed by 10 μm of cobalt, the rear-side $K\alpha$ emission of which is measured. The PE layer prevents fast electrons from reaching the cobalt. Comparing the cobalt $K\alpha$ emission with that of nickel, which is not photopumped by copper $K\alpha$ shows enhancement by almost a factor of 2.

PACS number(s): 52.40.Nk, 52.60.+h, 52.70.La

I. INTRODUCTION

It is well known that suprathermal electrons are generated when a high-intensity laser beam interacts with a solid target [1–5]. The advent of fs CPA lasers [6,7] allows investigation of this process at significantly higher intensities than previously possible. The most favorable conditions for hot electron generation occur when *p*-polarized laser pulses are obliquely incident on the target. In this case, collisionless mechanisms such as Brunel heating and resonance absorption lead to efficient coupling of laser pulse energy into the plasma electrons [8–13]. A small preplasma generated by an appropriate prepulse is advantageous for optimizing the absorption [14]. Due to the hot electrons, the emission from mid-*Z* materials is found to consist predominantly of $K\alpha$ photons and lines of highly ionized species are much reduced in the spectrum [15].

The $K\alpha$ radiation thus generated has been used to investigate ultrafast phenomena in semiconductors and Langmuir-Blodgett films [16–18]. A different suggestion involves pumping of an innershell x-ray laser [19–22]. This application requires a pumping material with a slightly higher nuclear charge than the material pumped to provide radiation above its *K* edge.

The hot-electron energy distribution is usually determined by the well-established technique of buried-layer x-ray emission [3,23–25]. Varying the layer thickness and recording the x-ray signal yields an indirect method of determining the hot-electron temperature. Typically, hot-electron temperatures determined in this way scale as $(I\lambda^2)^\alpha$ with an α between 1/3 and 1/2 and an absolute value of the hot-electron temperature of about 100 keV at $I\lambda^2 = 10^{17}\,\mathrm{W\,cm^{-2}}\,\mu\mathrm{m}^2$ [5,26,27]. This scaling approximately holds up to intensities exceeding $10^{19}\,\mathrm{W/cm^2}$ [24].

This study goes one step further to determine the electron energy distribution as well as other features of the electron beam generated, such as its global and differential directionality. Furthermore, the information obtained is used to design an experiment in which photopumping of $K\alpha$ radiation is demonstrated.

We use the rear-side emission from layered Cu/Ni targets irradiated by fs titanium-sapphire laser pulses at an intensity of $2\times10^{18}\,\mathrm{W/cm^2}$. Information on the electrons generated is obtained by matching the experimental data to Monte Carlo electron-photon transport simulations. Absolute calibration of the detector allows determination of the efficiency at which hot electrons are generated.

The experimental data are compared with those obtained with PIC code simulations. Both experiment and theory result in an electron energy distribution which can be described by two temperatures, a ''warm'' electron population with a temperature significantly below 100 keV and a ''hot'' electron population with an electron temperature of 200 keV.

After the electrons were characterized in this way, an experiment for demonstrating photopumping of cobalt innershell radiation by copper $K\alpha$ is conducted. The target designed for this purpose consists of three layers, a 10 μm thick copper foil, a 1 mm polyethylene (PE) layer, and a 10 μm cobalt or nickel backing layer. The middle PE layer is used to block the hot electrons from reaching the cobalt or nickel foils. Comparing the $K\alpha$ emission of cobalt to that of nickel shows enhancement of the cobalt emission by a factor of 1.75, a clear indication of photopumping.

II. EXPERIMENT

Experiments were conducted with the arrangement shown in Fig. 1. The ATLAS titanium-sapphire laser at MPQ has a power of 2 TW with a pulse duration of 130 fs. The laser pulses were focused *p*-polarized on solid targets by means of an off-axis parabola. The peak intensity reached at best focus was $2\times10^{18}\,\mathrm{W/cm^2}$. The laser pulse has a small spurious

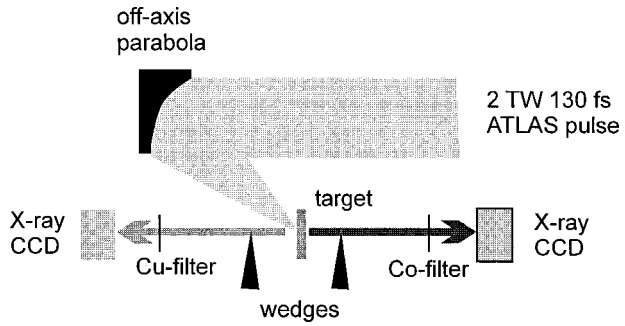

FIG. 1. Experimental arrangement used for generating and detecting hot electrons. 2 TW titanium-sapphire pulses are focused on the targets by means of an off-axis parabola. The x-ray emission is monitored by two CCD cameras observing the front and rear-side emission. To obtain spatial resolution, a stainless-steel wedge is inserted between the emitter and the CCD. A 100 μm beryllium filter blocks soft x rays. The CCD used to detect rear-side nickel $K\alpha$ emission has a 15 μm cobalt filter; the other CCD for copper $K\alpha$ has a 10 μm copper filter.

prepulse which generates a preplasma with a scale length $L/\lambda \approx 0.7-0.8$ [28]. An x-ray CCD in the energy readout mode [15] was used for spectrally resolved detection with a resolution of 200 eV, sufficient to separate the $K\alpha$ lines of the different materials. To obtain a spatially resolved image of the x-ray emission, a steel wedge was inserted between the target and detector, a magnification of 25 being used. The penumbral image of the emission recorded by the x-ray CCD was then used to deduce its spatial extent.

The targets used for characterizing the electrons consisted of copper foils of various thicknesses, backed by a thin nickel foil. Nickel is not photopumped by copper $K\alpha$ radiation and its emission thus serves as an indicator of the electrons arriving at the back of the copper foil. We found that the data were better reproducible if the targets were not made simply by pressing two foils onto each other. In this case a small gap between the copper and nickel layers is unavoidable and induces spurious space charge effects. The targets were therefore fabricated by galvanically depositing one material on the other. For the thin copper targets up to 25 μm the copper layer was deposited galvanically on a 10 μm nickel foil. For the thicker copper layers (copper thickness up to 46 μm) 6 μm of nickel was deposited on the respective copper foil.

The results obtained for the intensity of nickel $K\alpha$ for the different copper thicknesses are shown in Fig. 2. The data include shots on pure nickel which smoothly connect with those on the thinnest copper layer of 2 μm, indicating that the electron populations generated on nickel and copper targets are quite similar. On going from pure nickel to a 10 μm copper layer the emission drops by a factor of about five, but from then on it decreases only slowly with increasing copper foil thickness. This observation suggests a two-temperature distribution of the electrons propagating into the cold material.

The spatially resolved measurements, shown in Fig. 3, involved copper foil thicknesses of up to 55 μm, backed by 10 μm of nickel. They show a spot which, after remaining approximately constant up to a copper foil thickness of 35 μm, significantly increases at 55 μm. Note that the initial

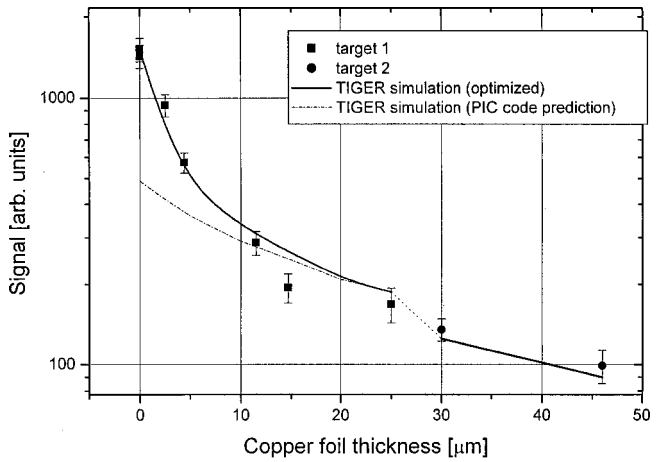

FIG. 2. Ni $K\alpha$ signal vs Cu foil thickness. Points labeled ''target 1'' and ''target 2'' are experimental. Target 1 has 10 μm of nickel on copper foil. Target 2 has 6 μm of nickel. The error bars include statistical shot-to shot fluctuation from 7 shots. The solid line is the result obtained from TIGER Monte Carlo simulations with the electron populations optimized to fit the data (97% 20 keV electrons and 3% 200 keV electrons). The dot-dashed line is obtained by using the PIC code result ($I_{\text{laser}} = 2\times10^{18}$ W/cm^2) in the TIGER simulations. Note that the initial steep drop is not reproduced by the distributions obtained from the PIC code.

$K\alpha$ spot size is already much larger than that of the laser pulse, which is consistent with previous results obtained for the front-side emission [29]. It is recalled that the larger spot size could only be partially explained by electrons generated in the low-intensity wings of the laser spot. Electric and magnetic fields forcing the electrons to travel along complicated orbits in front of the target may be responsible, but further study is required for complete clarification.

To determine the global direction of the electron beam generated, we made a series of shots in which we monitored the front and the rear-side emission from the targets. For this purpose, a second CCD was placed in front of the target and used to control the position of the front-side emission from the copper foil. This was necessary to correct for any lateral deviations resulting from small shot-to-shot fluctuations of the direction of the laser beam.

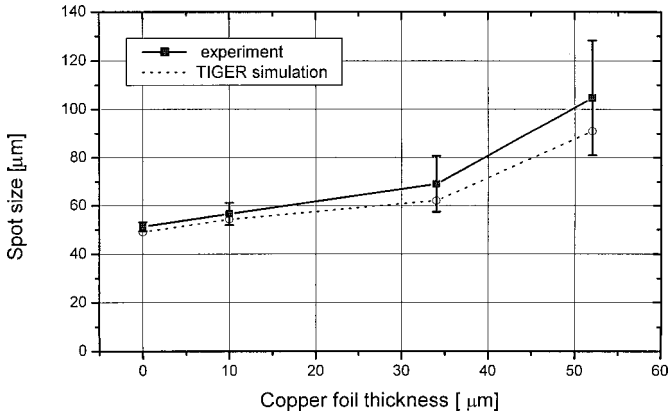

FIG. 3. Spot size (FWHM) of the rear-side Ni $K\alpha$ emission. Error bars denote shot-to-shot fluctuation from 5 shots. The result from the TIGER simulation uses the optimized electron temperature distribution. Electrons are emitted into a solid angle of 30°.

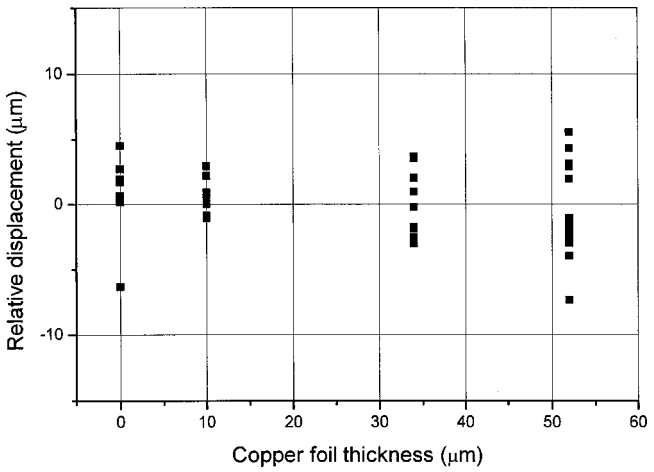

FIG. 4. Relative displacement of x-ray-emitting spot on the rear side vs copper foil thickness.

The result obtained in this experiment is shown in Fig. 4. The figure displays the relative spatial coordinate of the nickel $K\alpha$ spot at the rear side of the Cu/Ni target as a function of the copper foil thickness. If the electrons stayed in line with the laser beam, the position of the x-ray-emitting spot at the nickel foil would move laterally with increasing foil thickness. On the other hand, electrons propagating perpendicularly to the target surface generate a spot with a fixed lateral position for various copper foil thicknesses. The data shown in Fig. 4 clearly demonstrate that the latter situation prevails.

III. CHARACTERIZING HOT-ELECTRON POPULATIONS

In order to derive electron energy distributions from the experimental data, Monte Carlo simulations of the propagation of electrons and photons in the solid material were carried out. For these simulations the TIGER/ITS Monte Carlo electron-photon transport code was used. The code originated from the ETRAN code of Berger and Seltzer [30]. We use version 3.0 of the ITS package, which was released in 1992. The code tracks individual electrons and treats all collisional and radiative interactions with cold material. Its use requires as input the electron energy distribution and direction of the electrons.

Inhibition of electron propagation by electric field effects [31] is found to play no role in the experiment because of the high conductivity of copper. However, a point of concern for simulating rear-side emission was the fact that electrons leaving the target may be pulled back by electric fields generated at the rear side of the target. To correct for this effect, the transmitted electron population obtained in a particular run was reinjected into the target in a correction run and the resulting emission added to that previously obtained. This correction turned out to be quite significant, resulting in an additional emission of, typically, about 40% of the total. However, since the *relative* amount of the correction was quite similar for the different targets, the electron temperatures obtained were not affected by the correction.

The flat tail of the intensity curve after 10 μm of copper is well matched by electrons with a temperature of 200 keV. The fit of the simulations to the experimental data is quite sensitive to lowering of the hot-electron temperature, reduction to 150 keV resulting in 35% lower emission with 46 μm of copper, well outside our error bar. The sensitivity to an *increase* in the hot-electron temperature is not so high: An electron temperature of 250 keV is still within our error bar, and 300 keV would be just at its edge.

Matching the steep drop with small copper foil thicknesses to the simulations requires an electron population with a much lower temperature. The best agreement with our measurements is obtained with an electron energy distribution consisting of a majority of electrons with a temperature of 20 keV and a fraction 3×10^{-2} of hot electrons with a temperature of 200 keV (see Fig. 2). The solid angle for these electrons was obtained by fitting the TIGER results to the experimental x-ray spot size, yielding an angle of emission of 30°. However, the fits to the intensities are not very sensitive to the emission angle.

An absolute calibration of the CCD was carried out to determine the efficiency at which the hot electrons are generated. For this purpose, the CCD was illuminated with a radioactive source of Fe^{55} emitting a calibrated amount of Mn^{55} $K\alpha$ radiation at 5.9 keV. The sensitivity at the energy of Ni $K\alpha$ ($h\nu=7.5$ keV) was deduced from the transmission of the field-free region and the absorption of the depletion layer of the CCD chip. We obtain an absolute number of 1.0×10^{9} Ni $K\alpha$ photons behind 46 μm of copper. The number of $K\alpha$ photons per electron obtained from the TIGER code then results in an absolute number of 8.9×10^{11} electrons with a temperature of 200 keV and an energy conversion efficiency of 14% into these electrons.

IV. PIC SIMULATIONS

The electron energy distribution obtained is compared with that from particle-in-cell modeling of our experiment. The one and a half–dimensional EUTERPE code [32,33] with two velocity components (ν_x=parallel, ν_y=perpendicular to the target normal) and one space coordinate (parallel to the target normal) was used. Oblique incidence of the laser radiation on the plasma is treated by means of the relativistic ''boost-frame'' transformation [34]. Initial electron and ion distributions were supposed to be Maxwellian with temperatures of several 100 eV. The ratio Am_p/Zm_e was assumed to be 11 000, with the atomic number of copper $A=63.5$ and a mean charge $Z=11$. We start from an exponential density profile, with a critical scale length $L=0.7\,\lambda_{\mathrm{laser}}$. Sin^2-shaped laser pulses with a full width at half maximum (FWHM) of 70 laser periods were used. The final electron energy distributions for intensities of 2×10^{18} and $2\times10^{17}\,\mathrm{W/cm^2}$ are shown in Fig. 5. Several groups of electrons with different temperatures can be distinguished. Besides the low-energy compound of ''thermal'' electrons, we find a group of ''warm'' electrons and a high-energy tail. For $2\times10^{18}\,\mathrm{W/cm^2}$ the ''warm'' temperature is 40 keV and the high-energy tail has a temperature of approximately 200 keV, in agreement with our experimental result.

The ''hot'' and ''warm'' electron temperatures as predicted by the simulations for different intensities are shown in Fig. 6. As expected, both temperatures decrease smoothly with decreasing laser intensity. This behavior suggests that the intensity distribution in the focus of our laser will result

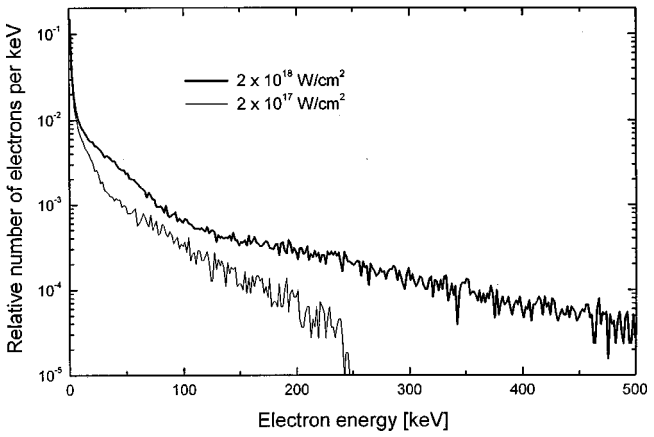

FIG. 5. Electron energy distributions as obtained by PIC code simulations. The curves exhibit two straight portions to which two temperatures can be ascribed.

in a higher population of ''warm'' electrons, as experimentally observed.

The particle diagnostic incorporated in the code allows one to analyze the ratio of the two particle momentum components p_x and p_y. Figure 7 displays the phase space $p_y(p_x)$ of all electrons with an energy >25 keV. In contrast to our experimental finding the transverse momentum is found to be nonzero, in particular for the high-energy part of the electrons. However, the axial momentum is observed to be considerably larger than the transverse momentum. Thus, the simulations are in partial agreement with our experimental finding that the hot electrons move predominantly perpendicularly to the target surface.

V. PHOTOPUMPING EXPERIMENT

The foregoing results were used to design an experiment to demonstrate photopumping of cobalt $K\alpha$ by copper K-shell radiation. The aim of this experiment is to show that hard x-ray photopumping can be clearly stronger than electron pumping of K-shell radiation. It is important in that inversion on innershell K-shell transitions can only be

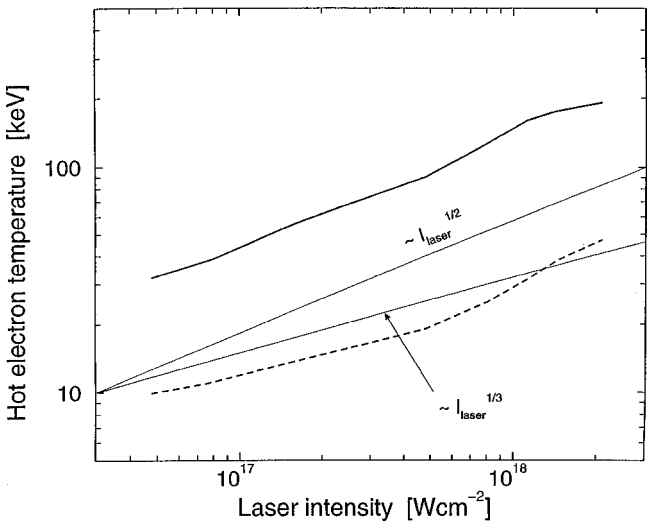

FIG. 6. Hot and ''warm'' electron temperatures vs intensity as predicted by PIC simulations.

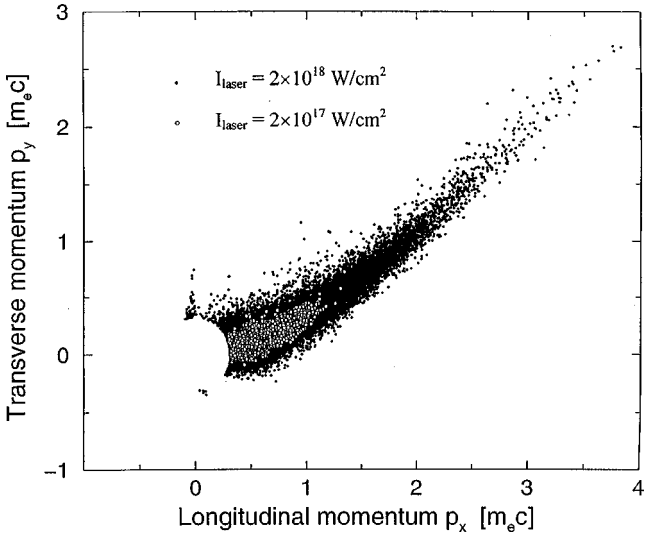

FIG. 7. Direction of the emitted electrons for 2×10^{17} and 2×10^{18} W/cm^2 as obtained from PIC simulations.

achieved by photopumping, whereas the electrons, due to their much larger cross section for the generation of L holes, invariably destroy the inversion [35].

For photopumping to be predominant, the number of electrons reaching the material to be photopumped should be as small as possible. To achieve this goal, we designed a target consisting of a 10μm copper foil (which maximizes the amount of copper $K\alpha$ emission from its rear side) followed by 1 mm of polyethylene (PE), finally backed by a 10 μm cobalt or nickel foil. Since nickel is not photopumped by copper $K\alpha$ emission, the cobalt-to-nickel ratio was used as a signature for the amount of photopumping. A ratio close to 1 means that K holes are generated mainly by hot electrons.

The thickness of the PE layer was chosen such as to block the main part of the 200 keV electrons. Using published data for the stopping power of PE [36], we expect that a 1 mm layer of this material should block electrons with an energy of up to 300 keV, while its transmission for copper $K\alpha$ radiation is about 70%.

The effect of the PE layer is quantified by TIGER simulations. Matching as closely as possible the geometry of our targets and the features of the electrons generated we obtain the results shown in Fig. 8. It is seen that the ''cold'' electron population, (which penetrates very little through the 10 μm copper foil and not at all through the thick PE) would generate a Co/Ni ratio of between 2 and 3.5, indicating predominant photopumping. On the other hand, the 200 keV electrons alone yield a ratio of around one. A simulation using the ''experimental'' two-temperature distribution obtained above yields a Co/Ni ratio of about 1.4 for 1 mm of PE. Without the PE layer the ratio would only be 1.19.

The result of the experiment is shown in Fig. 9, which displays the spectra obtained with the cobalt and nickel backing. Comparison of the two shows an enhancement of the Co $K\alpha$ emission with respect to the Ni $K\alpha$ emission of 1.75, somewhat higher than the value obtained with the TIGER runs. To explain the discrepancy it is recalled that the TIGER calculations take only collisional effects into account, but electron propagation through the PE plate may be inhibited by electric field effects [31].

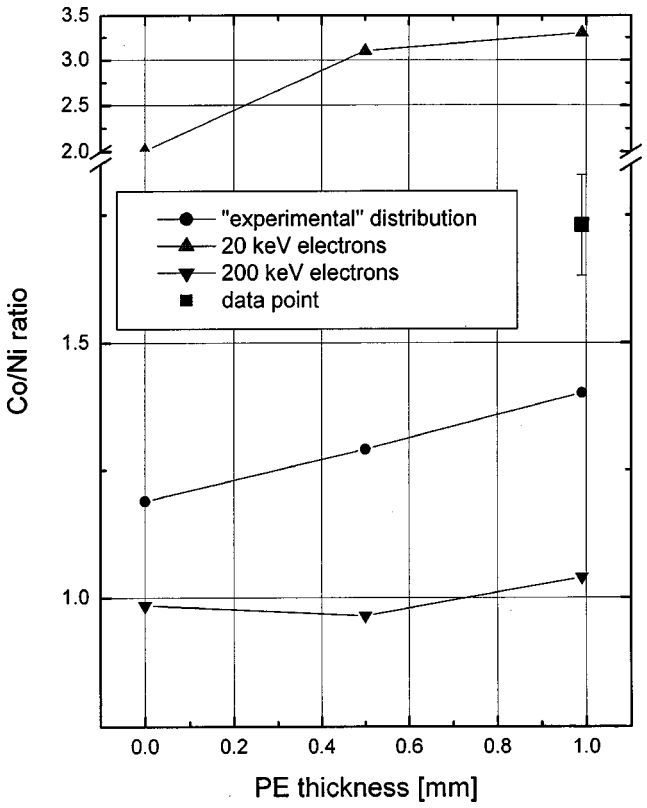

FIG. 8. Co/Ni $K\alpha$ emission ratio for CH layer thicknesses 0, 0.5, and 1 mm as predicted by TIGER simulations. Results are shown for 20 keV electrons, 200 keV electrons, and the ''experimental'' distribution comprising 3% of 200 keV electrons. Note that the 20 keV results are above an axis break. The experimental data point is also shown.

While a high Co/Ni $K\alpha$ ratio is certainly a signature for photopumping, let it be said that this ratio is not identical to the ratio of photopumped to electron-pumped emission. Analysis of the TIGER simulation results shows that about 25% of the nickel $K\alpha$ emission is generated by bremsstrahlung and is therefore also photopumped. A lesser amount is pumped by copper $K\beta$ radiation which is just above the nickel K edge. The TIGER code can be used to estimate what

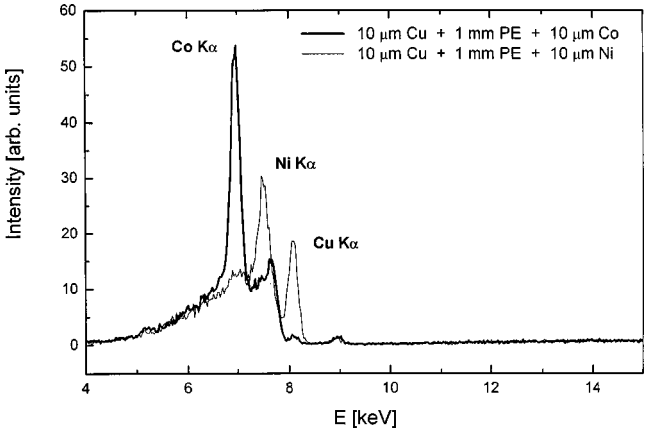

FIG. 9. Experimental spectra behind sandwich target with cobalt and nickel backing. The higher emission of Co $K\alpha$ clearly indicates photopumping. Cu $K\alpha$ pump line shines through nickel target but is absorbed by cobalt.

percentage of K holes is still directly generated by the electrons. This analysis shows that in cobalt this fraction is 47%, whereas in nickel it is 72%. Electric field effects mentioned above further reduce these numbers. Thus even in nickel a substantial amount of the $K\alpha$ photons generated is due to photopumping.

VI. CONCLUSION

The hot electrons generated upon interaction of a 130 fs pulse with a solid copper target have been characterized. With p-polarized pulses at an angle of incidence of 45° an electron population is generated which can be described by two temperatures, a relatively low one of 20 keV and a fraction of 3% of the electrons with a temperature of 200 keV Monte Carlo electron-photon transport simulations using this electron energy distribution reproduce well the intensities and spot sizes of the $K\alpha$ radiation generated in a thin nickel foil backing copper foils of various thicknesses. The absence of a shift in the lateral position of the rear-side spot with increasing copper foil thickness shows that the electrons are emitted perpendicularly to the target surface.

These findings are in partial agreement with PIC code simulations. The PIC simulations result in a two-temperature distribution the hot part of which (200 keV) agrees well with the ''experimental'' data. However, the low-temperature (''warm'') electrons are predicted to have a temperature of 40 keV with an approximately equal fraction of hot and ''warm'' electrons. The discrepancy between PIC simulations and the ''experimental'' electron energy distribution is explained by the distribution of intensities around the focus of our laser beam.

Furthermore, the PIC simulations predict that the main part of the electrons generated propagates perpendicularly to the target surface, in agreement with experiment. A smaller part, especially at the high-energy tail, however, is predicted to deviate from the target normal, a fact not reproduced by the experiment.

The ''experimental'' distribution obtained for the electrons is used to design an experiment demonstrating photopumping of cobalt using copper $K\alpha$ radiation as the pump. The target contains a 1 mm thick PE layer which prevents the electrons from reaching the medium to be photopumped. This yielded a factor of 1.75 enhancement of the cobalt radiation in relation to nickel, which is not photopumped by copper $K\alpha$. The simulations predict a smaller enhancement factor, which can be explained by self-generated electric fields inhibiting electron propagation in a dielectric. The analysis shows that more than 50% of the cobalt $K\alpha$ radiation is generated by photopumping.

ACKNOWLEDGMENTS

A. Böswald and H. Haas are thanked for ensuring reliable operation of the ATLAS laser and W. Fölsner for fabricating the targets. We thank R. Volk for help with the installation of the TIGER code. This work was supported in part by the Commission of the European Communities within the framework of the Euratom/Max-Planck-Institut für Plasmaphysik Association. D.E. was supported by the Alexander von Humboldt Foundation and the U.S. DOE under LLNL Contract No. W-7405-ENG-48.

[1] D. W. Forslund, J. M. Kindel, and K. Lee, Phys. Rev. Lett. **39**, 284 (1977).
[2] S. J. Gitomer, R. D. Jones, F. Begay, A. W. Ehler, J. F. Kephart, and R. Kristal, Phys. Fluids **29**, 2679 (1986).
[3] B. Luther-Davies, A. Perry, and K. A. Nugent, Phys. Rev. A **35**, 4306 (1987).
[4] U. Teubner, I. Uschmann, P. Gibbon, D. Altenbernd, E. Förster, T. Feurer, W. Theobald, R. Sauerbrey, G. Hirst, M. H. Key, J. Lister, and D. Neely, Phys. Rev. E **54**, 4167 (1996).
[5] F. N. Beg, A. R. Bell, A. E. Dangor, C. N. Danson, A. P. Fews, M. E. Glinsky, B. A. Hammel, P. Lee, P. A. Norreys, and M. Tatarakis, Phys. Plasmas **4**, 447 (1997).
[6] P. Maine, D. Strickland, P. Bado, M. Pessot, and G. Mourou, IEEE J. Quantum Electron. **24**, 398 (1988).
[7] G. A. Mourou, C. P. J. Barty, and M. D. Perry, Phys. Today **51**, 22 (1998).
[8] F. Brunel, Phys. Rev. Lett. **59**, 52 (1987).
[9] P. Gibbon, Phys. Rev. Lett. **73**, 664 (1994).
[10] A. Rousse, P. Audebert, J. P. Geindre, F. Falliès, J. C. Gauthier, A. Mysyrowicz, G. Grillon, and A. Antonetti, Phys. Rev. E **50**, 2200 (1994).
[11] H. Ruhl, Y. Sentoku, K. Mima, K. A. Tanaka, and R. Kodama, Phys. Rev. Lett. **82**, 743 (1999).
[12] M. Tatarakis, J. R. Davies, P. Lee, P. A. Norreys, N. G. Kassapakis, F. N. Beg, A. R. Bell, M. G. Haines, and A. E. Dangor, Phys. Rev. Lett. **81**, 999 (1998).
[13] L. A. Gizzi, D. Giulietti, A. Giulietti, P. Audebert, S. Bastiani, J. P. Geindre, and A. Mysyrowicz, Phys. Rev. Lett. **76**, 2278 (1996).
[14] J.-C- Gauthier, S. Bastiani, P. Audebert, J.-P. Geindre, A. Rousse, C. Quoix, G. Grillon, A. Mysyrowicz, A. Antonetti, R. Mancini, and A. Shlyaptseva, Proc. SPIE **3157**, 52 (1997).
[15] J. Dunn, B. K. F. Yound, and S. J. Shiromizu, Rev. Sci. Instrum. **66**, 706 (1995).
[16] C. Rischel, A. Rousse, I. Uschmann, P. A. Albouy, J.-P. Geindre, P. Audebert, J.-C. Gauthier, E. Förster, J.-L. Martin, and A. Antonetti, Nature (London) **390**, 490 (1997).
[17] C. Rose-Petruck, R. Jimenez, T. Guo, A. Cavalleri, C. W. Siders, F. Raksi, J. A. Squier, B. C. Walker, K. R. Wilson, and C. P. J. Barty, Nature (London) **398**, 310 (1999).
[18] C. Siders, A. Cavalleri, K. Sokolowski-Tinten, T. Guo, C. Toth, R. Jimenez, C. Rose-Petruck, M. Kammler, M. Horn von Hoegen, D. von der Linde, K. R. Wilson, and C. P. J. Barty, in *Soft X-ray Lasers and Applications III*, edited by J. J. Rocca and L. Da Silva, Proc. SPIE Vol. 3776 (SPIE, Bellingham, WA, 1999), pp. 302–311.
[19] E. Fill, D. Eder, K. Eidmann, J. Meyer-ter-Vehn, G. Pretzler, A. Pukhov, and A. Saemann, in *X-ray Lasers 1998*, edited by Y. Kato, H. Takuma, and H. Daido, Inst. Phys. Conf. Ser. No. 159 (Institute of Physics, Bristol, 1999), pp. 301–308.
[20] E. Fill, G. Pretzler, D. Eder, K. Eidmann, and A. Saemann, in *Soft X-ray Lasers and Applications III* (Ref. [18]), pp. 110–117.
[21] S. J. Moon and D. C. Eder, Phys. Rev. A **57**, 1391 (1998).
[22] M. A. Duguay and P. M. Rentzepis, Appl. Phys. Lett. **10**, 350 (1967).
[23] J. D. Hares, J. D. Kilkenny, M. H. Key, and J. G. Lunney, Phys. Rev. Lett. **42**, 1216 (1979).
[24] K. B. Wharton, S. P. Hatchett, S. C. Wilks, M. H. Key, J. D. Moody, V. Yanovsky, A. A. Offenberger, B. A. Hammel, M. D. Perry, and C. Joshi, Phys. Rev. Lett. **81**, 822 (1998).
[25] S. Bastiani, P. Audebert, J. P. Geindre, Th. Schlegel, J. C. Gauthier, C. Quoix, G. Hamoniaux, G. Grillon, and A. Antonetti, Phys. Rev. E **60**, 3439 (1999).
[26] J. R. Davies, A. R. Bell, M. G. Haines, and S. M. Guérin, Phys. Rev. E **56**, 7193 (1997).
[27] P. Gibbon and E. Förster, Plasma Phys. Controlled Fusion **38**, 769 (1996).
[28] M. Zepf, G. D. Tsakiris, G. Pretzler, I. Watts, D. M. Chambers, P. A. Norreys, U. Andiel, A. E. Dangor, K. Eidmann, C. Gahn, A. Machacek, J. S. Wark, and K. Witte, Phys. Rev. E **58**, R5253 (1998).
[29] D. C. Eder, G. Pretzler, E. Fill, K. Eidmann, and A. Saemann, Appl. Phys. B: Lasers Opt. **70**, 211 (2000).
[30] S. M. Seltzer, Appl. Radiat. Isot. **42**, 917 (1991).
[31] A. R. Bell, J. R. Davies, S. Guerin, and H. Ruhl, Plasma Phys. Controlled Fusion **39**, 653 (1997).
[32] G. Bonnand and G. Reisse, Nucl. Fusion **26**, 633 (1986).
[33] Th. Schlegel, S. Bastiani, I. Grémillet, J.-P. Geindre, P. Audebert, L.-C. Gauthier, E. Lefebre, G. Bonnaud, and J. Delettrez, Phys. Rev. E **60**, 2209 (1999).
[34] A. Bourdier, Phys. Fluids **26**, 1804 (1983).
[35] E. E. Fill, Opt. Commun. **162**, 233 (1999).
[36] L. Pages, E. Bertel, H. Joffre, and L. Sklavenitis, At. Data **4**, 1 (1972).